https://doi.org/10.5194/egusphere-2026-290
Preprint. Discussion started: 4 February 2026

Parameter estimation of river incision models of soft sedimentary rocks — a case study on the Kamikita Coastal Plain, northeast Japan

Shizuka Takai[1], Tomoji Sanga[2], Taro Shimada[1], Seiji Takeda[1]

[1]Nuclear Safety Research Center, Japan Atomic Energy Agency, Ibaraki, 319-1195, Japan
[2]SNG Consultant, Saitama, 335-0013, Japan

Correspondence to: Shizuka Takai (takai.shizuka@jaea.go.jp)

Abstract. To predict long-term future landscape evolution, understanding of the river incision model, which is the main driver of continental erosion, is especially important. For the bedrock channel incision model (detachment-limited (DL) model: erosion rate $E = KA^mS^n$ where A is drainage area, S is channel gradient, and K, m, n are parameters), parameters can be estimated by the slope-area analysis if E is known. Based on the worldwide basin-averaged denudation rates of ^{10}Be concentrations, previous studies compiled the parameter values for variable lithology. However, the scarcity of data for the soft sedimentary rock limits the applicability of global scale compilation. In addition, measuring the ^{10}Be concentration in sedimentary rock is difficult in humid and tectonically active regions like Japan. To address this, slope-area analysis was conducted in the Kamikita Coastal Plain, Japan, where bedrock lithology (sedimentary rocks of Miocene to Pleistocene) and uplift rate (~ 0.2 mm y^{-1} for the past 300 ka) are assumed to be uniform. Parameter values were estimated based on river incision rates approximately derived from marine terraces (MIS 5e, 7, 9, and 11) which are widely distributed in the area. For six target rivers, DL-like behaviour was confirmed in the limited upstream and midstream areas located upstream of the alluvium distribution. Except for small rivers of $A < 25$ km^2, the concavity index m/n was between 0.35 and 0.6, which is the typical range for steady-state channels. The estimated exponent n was nonlinear, ranging between 1 and 2, which is consistent with the previous global compilations. This nonlinearity can be explained by past sea-level changes causing knickpoints at similar elevations. Finally, the erosion coefficient K was estimated to be $10^{-5\sim-6}$ m$^{0.1}$ y^{-1}. For the main lithology of late Pliocene and early Pleistocene sedimentary rock, the estimated K almost agreed with the global relationship between K and unconfined compressive strength q_u ($K \propto 1/q_u^2$), supporting the significant influences of bedrock lithology on K.

1 Introduction

Prediction of long-term future landscape evolution is indispensable for social planning such as radioactive waste disposal and mine waste disposal. For example, the disposal facility for intermediate or high-level radioactive waste must be evaluated to ensure that it will remain isolated from the biosphere and humans for at least several thousand years (IAEA, 2011) to one million years (STUK, 2013). Among various landscape processes, river incision is one of the main drivers of landscape evolution and can cause large vertical erosion. Therefore, a quantitative understanding of river incision models and their parameters is essential for making long-term projections of erosion depth.

River incision models are broadly classified into two types: the detachment-limited (DL) model and the transport-limited (TL) model. The DL model assumes that all particles eroded by the river are immediately removed from the system. The long-term river incision rate E [L T^{-1}] is controlled by shear stress or stream power per unit width on the bed (e.g., Howard and Kerby, 1983; Howard, 1994; Whipple and Tucker, 1999). Under idealized circumstances, E is described as a simple function of both channel slope S [-] and upstream drainage area A [L^2] as follows:

$$E = KA^mS^n , \quad (1)$$

where m and n are positive constants ($\theta = m/n$ is the concavity index). K [L^{1-2m} T^{-1}] is the erosion coefficient reflecting the combined influences of bed erodibility, climate and downstream changes in channel hydraulic geometry. On the other hand,

https://doi.org/10.5194/egusphere-2026-290
Preprint. Discussion started: 4 February 2026

the TL model assumes that sediment flux Q [L^2 T^{-1}] transported by the river is limited by its transport capacity (Henderson, 1966; Hergarten, 2020):

$$Q \propto A^{m+1} S^n . \quad (2)$$

The values of S and A can be easily calculated based on digital elevation model (DEM). Therefore, if E is known and the environment (i.e., tectonics, lithology, and climate) is uniform, the river incision parameters (m, n, and K) can be estimated from the field data and the DL model. When using data from rivers with different drainage areas, a reference concavity θ_{ref}, generally the regional mean of observed θ, is used for comparison purposes.

In recent decades, river incision parameters have been estimated in various regions (e.g., Kirby and Whipple, 2012; Lague, 2014; Harel et al. 2016; Hilley et al., 2019; Adams et al., 2020; Desormeaux et al., 2022; Hu et al., 2023; Marder and Gallen, 2023; Ott et al., 2023) and global compilations have been conducted using this data. For example, Lague (2014) estimated the parameters for 10 basins globally distributed and found that $n \sim 2$ (ranging from 1 to 4) using $\theta_{ref} = 0.45$. Harel et al. (2016) compiled the parameter values at 59 study areas of various lithology, climatic, and tectonic settings. Using $\theta_{ref} = 0.5$, a mean (±1σ) n of 2.7 (±2.9) was suggested. Moreover, Haag and Schoenbohm (2025) indicated that the global compiled K in Harel et al. (2016) is inversely proportional to the square of unconfined compressive strength q_u: $K \propto 1/q_u^2$.

However, there are two problems with the above studies. First, previous research ($q_u \geq 15$ MPa: Haag and Schoenbohm, 2025) lacks data of soft sedimentary rocks. This is especially important for Japan where over 50% of the surface geology consists of Paleogene and Neogene sedimentary rocks (NUMO, 2021). Nevertheless, river incision parameters and its relationship with q_u have not been discussed for soft sedimentary rocks with q_u = 1–10 MPa. Second, previous parameter estimations have primarily relied on basin average denudation rates derived from cosmogenic beryllium-10 (^{10}Be) in quartz grains from river sediments. However, it is difficult to measure the ^{10}Be concentration for sedimentary rocks in humid and tectonically active regions like Japan due to the lack of quartz and the diversity of topographic deformation and sedimentation-erosion processes (AIST, 2016). In such regions, the ^{10}Be measurement is appropriate for quartz-rich rocks, such as granite (e.g., Takahashi et al., 2023). Parameter estimations have been also conducted assuming a topographic steady state (e.g., Snyder et al., 2000; Kirby and Whipple, 2001; Duvall et al., 2004). However, many environments have not yet attained a steady state (Bishop et al., 2005; Campforts and Govers, 2015; Vanacker et al., 2015; Armitage et al., 2018). Especially in coastal areas, which are preferable for geological disposal in terms of safe waste transportation (METIJ, 2017), the landscape has been drastically changed due to periodic sea-level change. Very a few studies (e.g., Lague, 2014) address this issue by using reach incision rates based on fluvial terraces.

To address these issues, we performed slope-area analysis in the Kamikita Coastal Plain, Japan, where bedrock lithology (sedimentary rocks of Miocene to Pleistocene) and uplift rate are assumed to be uniform. Parameter values were estimated based on river incision rates approximately derived from marine terraces (Marine Isotope Stages (MIS) 5e, 7, 9, and 11) widely distributed in the area. First, we estimated the validity range of the DL model and θ for six target rivers. Then, we estimated the river incision parameters using the erosion rates approximately evaluated from the marine terraces. Finally, we confirmed the validity of the estimated parameter values by comparing them with those from previous global compilations.

https://doi.org/10.5194/egusphere-2026-290
Preprint. Discussion started: 4 February 2026

2 Study area

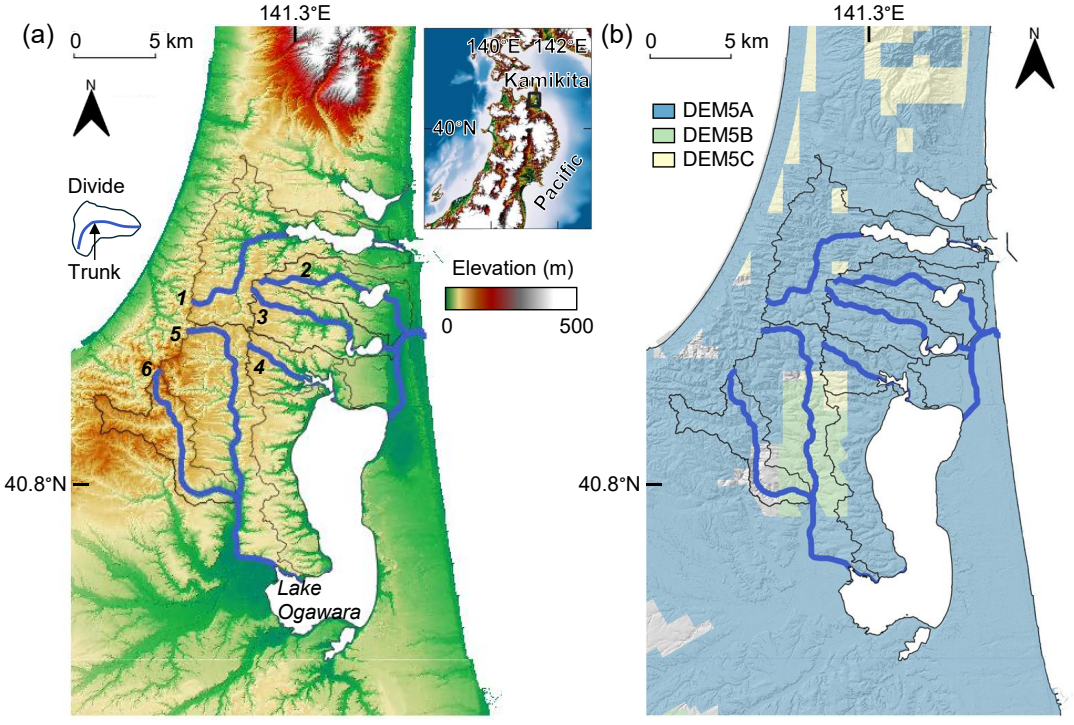

Figure 1: (a) Topography and (b) provided area of 5 m DEM by Geospatial Information Authority of Japan. For area where 5 m DEM is not provided, 10 m DEM was used.

The Kamikita Plain in northeast Japan is a vast coastal plain approximately 30 × 50 km^2, located along the coastline of Pacific Ocean (Fig. 1a). In this region, Middle and Late Pleistocene marine terraces are widely preserved at multiple levels (Fig. 2a): the Takadate terrace (MIS 5e), the Tengudai terrace (MIS 7), the Shichihyaku terrace (MIS 9), and the higher terrace (MIS 11) (AIST, 2016). The chronology has been estimated using various techniques: sediment rate chronology (Miyauchi, 1985; Koike and Machida, 2001), optically stimulated luminescence (AIST, 2015, 2016), and tephra and phytolith stratigraphy (Kuwabara, 2004, 2007, 2009; Matsu'ura et al., 2019). Based on these previous studies, Matsu'ura et al. (2019) concluded that the uplift rate of the Kamikita Plain (around Lake Ogawara) has been constant at approximately 0.2 mm y^{-1} over the last 300 ka.

Geological units of the Kamikita Plain are summarised by Kudo et al. (2020) (Fig. 2b). Bedrock was formed in the early to middle Miocene: the Takahoko Formation, sedimentary rock (16.6–13.1 Ma), and the Tomari Formation, volcanic rock (16.6–15 Ma). Sedimentary rock of late Pliocene to early Pleistocene, the Hamada formation and the Katchi formation, overlies the bedrock. These sedimentary rocks are covered by terrace deposits of middle to late Pleistocene and alluvium. The mean annual rainfall in this region is around 1,300 mm (JMA, 2026).

https://doi.org/10.5194/egusphere-2026-290
Preprint. Discussion started: 4 February 2026

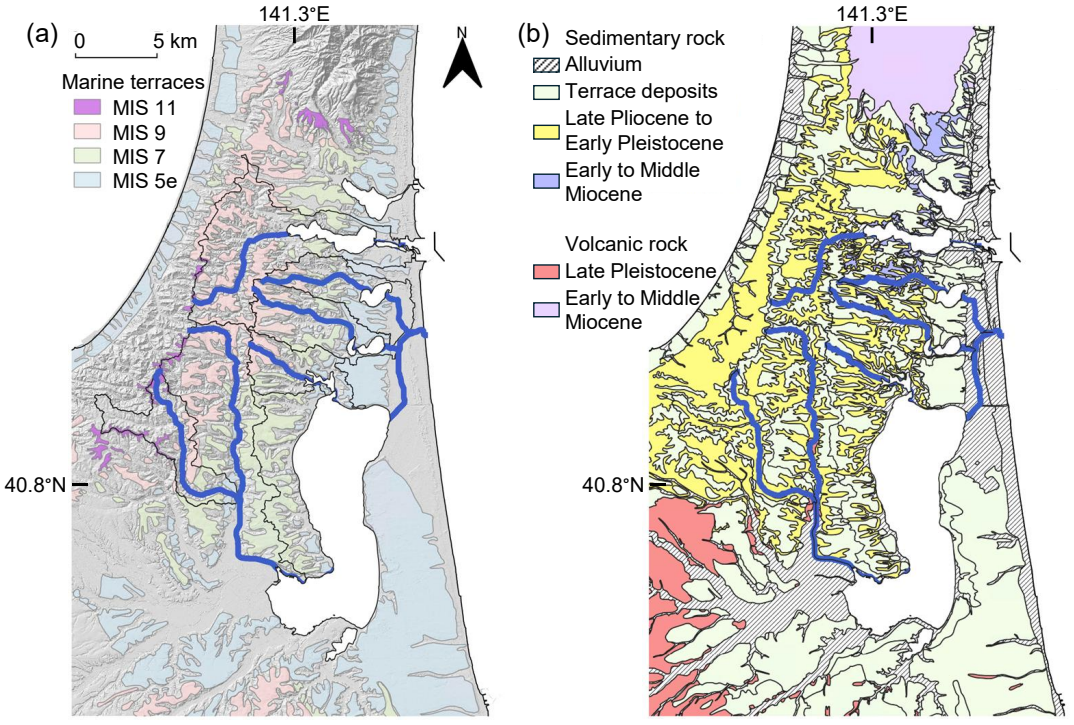

Figure 2: (a) Marine terraces and (b) geology of the study area. Marine terraces are based on Koike and Machida (2001). Geological map is based on the 1:200,000 scale geologic map (AIST, 2025). Geological units are based on Kudo et al. (2020).

The Continental Divide is located in the western part of the study area. The valley is deep on the west side of the divide and shallow on the east side. The rivers on the east side dissect the marine terraces and flow into the Pacific Ocean. Downstream the rivers, coastal lagoons such as Lake Ogawara are located, which were formed by sea-level fall during the Last Glacial Maximum and by subsequent development of sandbanks during the post-glacial period. In this study, we examined six streams flowing into the Pacific Ocean (1: the Togusari River, 2: the Ishiwatari River, 3: the Hiranuma River, 4: the Uchinuma River, 5: the Doba River, 6: the Gandosawa River) (Table 1), whose lithologic (sedimentary rock of Miocene to Pleistocene) and tectonic conditions (uplift rate ~ 0.2 mm y^{-1}) can be assumed to be uniform. Note that the rivers No. 2–6 are tributaries of the Takase River, which flows from the Hakkoda Mountains located west of the study area. Volcanic rocks are distributed throughout the region and the tectonics differ from that of the Kamikita Plain; therefore, the Takase River was excluded from the scope of this study.

Table 1: Target rivers. Drainage area and length include coastal lagoons.

No.	River	Drainage Area (km^2)	Length (km)	Valley-head elevation (m)
1	Togusari River	55.9	18.7	64.8
2	Ishiwatari River	23.0	12.9	67.9
3	Hiranuma River	24.6	12.7	74.7
4	Uchinuma River	16.2	7.1	63.7
5	Doba River	74.4	22.2	73.5
6	Gandosawa River	74.4	20.2	93.5

https://doi.org/10.5194/egusphere-2026-290
Preprint. Discussion started: 4 February 2026

3 Methods

As previous research has shown (e.g., Whipple and Tucker, 2002; Whipple, 2004), most bedrock channels are mixed bedrock-alluvial channels partially covered by alluvium. In this case, the river profile consists of colluvial, bedrock, and alluvial sections (Fig. 3a). In the bedrock section where the DL model holds, Eq. (1) can be rewritten as the stream power law (Hack, 1957; Flint, 1974):

$$S = k_s A^{-\theta} , \quad (3)$$

where $k_s = (E/K)^{1/n}$ [$L^{2\theta}$] is the steepness index. This means that in the DL model, the log-transformed slope-area plot can be fitted with a linear regression (Fig. 3b). Since channel transitions from bedrock to alluvial (i.e., DL to TL) or colluvial processes typically cause changes in channel slope (e.g., Whipple and Tucker, 1999, 2002; Stock et al., 2005), sections can be identified using the slope-area plot (Wang et al., 2017). Above a critical drainage area (A_c), colluvial processes, such as debris flows and land sliding, are dominant (Wobus et al., 2006). Below A_c, the fluvial processes dominate. Both the bedrock and alluvial sections exhibit a descending gradient with increasing drainage areas (Whipple and Tucker, 2002). However, the transition to alluviated conditions cause a sudden reduction in channel gradient (Wobus et al., 2006).

Channels may contain knickpoints, which can be classified into two categories: vertical-step knickpoints and slope-break knickpoints (Fig. 3c). Vertical-step knickpoints correspond to sudden changes in elevation, such as waterfalls, and can be identified as spikes on the slope-area plot. These knickpoints are generally caused by channel-scale heterogeneities such as bounding faults (e.g., Kirby and Whipple, 2012; Liu et al., 2020). Slope-break knickpoints, on the other hand, develop spatially or temporally, which corresponds to regional-scale trends of lithologic heterogeneity and sea-level fall (e.g., Haviv et al., 2010; Kirby and Whipple, 2012; Boulton et al., 2020). In this study, we focused on the slope-break knickpoints, which cause an abrupt change in flow condition.

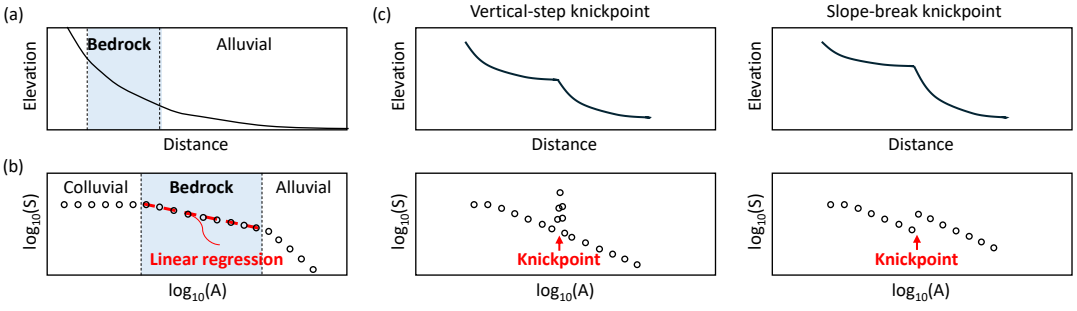

Figure 3: Schematic of (a) river profile, (b) slope-area plot, and (c) knickpoints (revised from Snyder et al. (2000) and Whipple (2013)).

This study estimated river incision parameters in three consecutive steps. First, sections exhibiting DL-like behaviours were identified from slope-area plots. Their validity was confirmed by comparing them with the alluvium distribution. We used a 5 m gridded digital elevation model (DEM), which is provided by the Geospatial Information Authority of Japan (Fig. 1b). Three types of 5 m DEM collected by different methods were combined: DEM5A (airborne LiDAR measurements), DEM5B and DEM5C (photogrammetry). There is also a 10 m DEM covering the entire country, which is created by interpolating topographic contour map with 10 m intervals. However, such a DEM can cause problems, such as artificial knickpoints due to interpolation errors or short-circuit meander bends in a river profile (Wobus et al., 2006). Therefore, we used the higher-resolution 5 m DEM. In areas where 5 m DEM is not available, such as the southeastern part of the Doba River and the middle of the Gandosawa River, 10 m DEM was bilinearly resampled to 5 m point spacing. Using the ArcHydrology toolbox (Tarboton

https://doi.org/10.5194/egusphere-2026-290
Preprint. Discussion started: 4 February 2026

et al., 1991), streams were extracted by applying a D8 flow routing algorithm and the trunk was defined from the Horton-Strahler number. To circumvent noise, previous research (Wobus et al., 2006; Whipple et al., 2007) has indicated that DEM-derived river profiles require the implication of some smoothing algorithms, such as a moving-window average. Furthermore, calculating the averaged channel slopes at a certain elevation interval or logarithmic bins of drainage area (log-bin averaging) was suggested (e.g., Snyder et al., 2000; Wobus et al., 2006). The measurement error (standard deviation) of the DEM is 0.3 m (DEM5A), 0.7 m (DEM5B), 1.4 m (DEM5C), and 5 m (10m DEM). In this study, we smoothed elevation data over a 500 m moving window and calculated averaged slopes on 5 m contours and log-bin averaged slopes.

In the second step, we calculated the channel concavity index from the integral approach (Perron and Royden, 2013):

$$\chi = \int_{x_b}^{x} \left(\frac{A_0}{A(x)}\right)^{\theta} dx \,, \tag{4}$$

$$z(x) = z(x_b) + \left(\frac{E}{K A_0{}^m}\right)^{1/n} \chi \,, \tag{5}$$

where x [L] is the horizontal upstream distance from an outlet; x_b [L] is the distance at the outlet (in this study, $x_b = 0$); and z [L] is elevation. The validity of the bedrock sections identified by slope-area plots is confirmed again by the linearity of χ plot. Using a reference basin area of $A_0 = 1$ m^2, we estimated θ as the value providing the best linear fit between χ and z. $k_{sn} = SA^{\theta_{ref}}$ was calculated using θ_{ref}, the regional mean of θ. Knickpoints were extracted as the local minimum points of k_{sn} with respect to χ (Gailleton et al., 2019).

In the third step, the values of n and K were estimated by regression analysis of logarithms of E and k_{sn} ($\ln(E) = a\ln(k_{sn}) + b$ where $a = n$, $b = \ln(K)$). River terraces are not identified in the study area (Koike and Machida, 2001). Since the target rivers incising marine terraces have smooth and concave-up profiles, long-term incision rate E was approximately calculated based on the height of marine terraces:

$$E = (z_t - z_r - d)/T_t \,, \tag{6}$$

where z_t [L] is the summit level of the marine terrace; z_r [L] is the present river profile; d [L] is the thickness of tephra and loess; and T_t [T] is the formation age of the river. T_t was approximated as the terrace age where valley head is located.

Due to volcanoes in the nearby districts, tephra layers and loam (tephric loess) intercalated with tephra layers of various ages are observed in the study area. The main tephra layers are as follows (Kudo, 2023): Hakkoda second-stage (Hkd2: 0.19–0.29 Ma) and White Pumice (WP: 210 ka) erupted form the Hakkoda Volcano; Orange Pumic (OrP: 166 ka) and Towada-Ofudo (To-Of: 36 ka) erupted from the Towada Volcano; and Toya (106 ka) erupted from the Toya Volcano. Based on outcrop observations at seven locations, AIST (2015, 2016) has identified the tephra and loam thickness as 11.4 m (sampled at Onadesawa) and 10.5 m at Kanaya for MIS 11; 14 m at Shichihyaku and 7 m at Kamiyoshita for MIS 9; 6 m at Hotozawa for MIS 7; 2 m or 4 m at Neinuma for MIS 5e. For the MIS 5e marine terraces, Koike and Machida (2001) indicated that the thickness of cover deposit layers are 2 m at four points to 3 m at one point. Based on previous research, d is assumed to be 12 m for MIS 11, 10 m for MIS 9, 5 m for MIS 7, and 2 m for MIS 5e terraces. Note that Kudo (2023) provides an approximate estimate of the spatial distribution of tephra thickness for the Towada Volcano. However, this information is not provided for other volcanoes. Therefore, we did not consider regional differences in the thickness of covering layers.

4 Results

4.1 Channel profiles

Longitudinal river profiles, slope-area plots, and χ plots for six rivers are shown in Fig. 4. A_{cr} is confirmed at ~ 0.1 km^2 for all rivers, which is consistent with earlier studies (e.g., Montgomery and Foufoula-Georgiou, 1993; Stock and Dietrich, 2003; Wobus et al., 2006). In the slope-area plots (Fig. 4b), all rivers exhibit an approximately linear descending gradient with

https://doi.org/10.5194/egusphere-2026-290
Preprint. Discussion started: 4 February 2026

increasing drainage areas. The gradients suddenly reduce around A = 1–10 km^2 upstream of the alluvium distribution. This is consistent with previous research on mixed bedrock and alluvial channels (Snyder et al., 2000; Wobus et al., 2006, Wang et al., 2017), reflecting a transition to alluviated conditions due to the sea level rise during the Holocene. Therefore, the studied rivers are considered to be mixed bedrock and alluvial channels, and the sudden decrease in the channel gradient corresponds to the transition from erosive bedrock channels (DL) to depositional alluvial channels (TL).

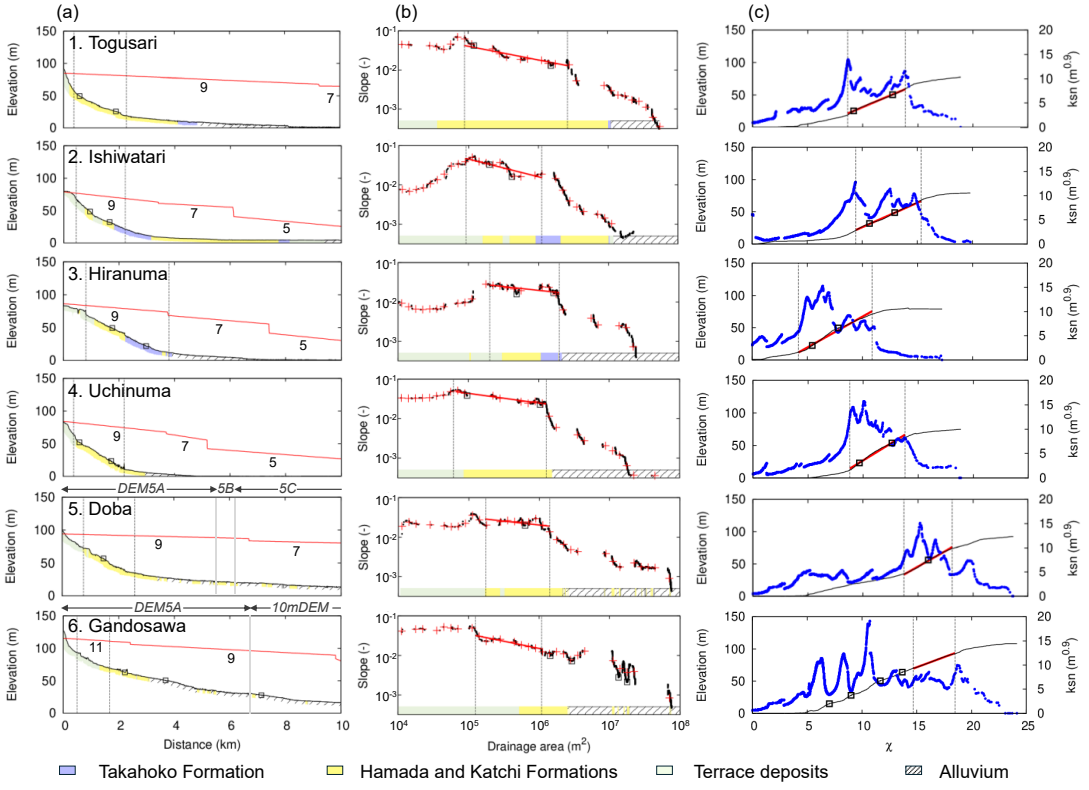

Figure 4: Stream profile analysis of the study area. (a) Longitudinal profile (black line) and the elevation of marine terraces (red line) with Marine Isotope Stages. Squares denote knickpoints. Gray lines for rivers No. 5 and 6 indicate the boundaries of DEMs other than DEM5A (LiDAR 5m DEM). (b) Slope-area plot. Average channel slopes are calculated on 5-m contours (black point) and by the log-bin averaging method (red mark). (c) χ plot (black line) based on the reference concavity (θ = 0.45) with k_{sn} (blue point).In all graphs, dashed lines and red bold lines correspond to the bedrock section and its regression line.

Estimated values of concavity index (θ) are summarised in Table 2. For all rivers, optimal θ achieved the linear regression of χ plots with high correlation coefficients of $R \sim 1$ (Fig. 5), which manifests DL-like behaviour in the upstream and midstream sections. Although θ ranges from 0.11 to 0.59, θ is approximately 0.4 except for small rivers of A < 25 km^2 (No. 2, 3, 4), which is the general range of steady-state channels (θ = 0.35–0.6: Kirby and Whipple, 2012). Notably, θ of river No. 6, whose formation age (MIS 11) is the oldest, is close to 0.45, a typical value for reference concavity index (e.g., Wobus et al., 2006). Snyder et al. (2003) indicates that even considering sea-level changes, a quasi-steady-state condition has been achieved in the upper parts of the channel. Therefore, although small channels tend to fluctuate from their mouths to their divides reflecting sea-level change, it can be assumed that the other rivers have approached to the quasi-steady state in the upstream section. In subsequent calculations, we analyzed k_{sn} based on θ_{ref} = 0.45.

https://doi.org/10.5194/egusphere-2026-290
Preprint. Discussion started: 4 February 2026

Table 2: Formation ages and concavity indices.

No.	1	2	3	4	5	6
Formation Age	MIS 9	MIS 9	MIS 9	MIS 9	MIS 9	MIS 11
θ	0.35	0.59	0.18	0.16	0.35	0.44

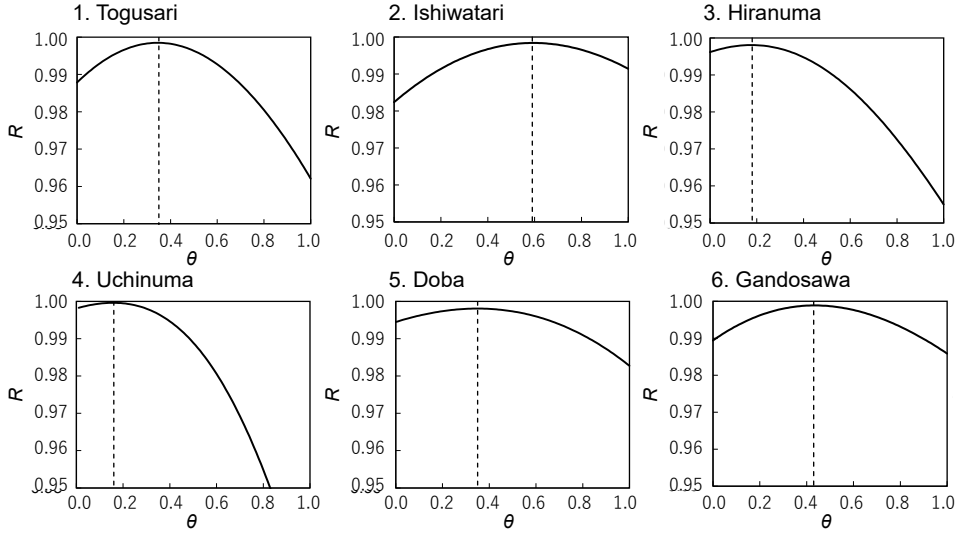

Figure 5: Correlation coefficients of χ plots based on a range of θ.

Figure 6 shows a map of the extracted knickpoints from the χ plots (Fig. 4c). The knickpoints are distributed at similar elevations (around E.L. 25 m and 50 m), which do not correspond to the lithology or the boundary of the different DEMs. This suggests that they can be base-level-fall related upstream-migrating knickpoints. In the Sanriku Coast, approximately 50 km south of the study area, Ogami (2015) indentified upstream-migrating knickpoints in multiple rivers which were formed during the sea-level highstands during MIS 5e, 7, 9, and 11. The knickpoints in the study area may have been formed for the same reason.

Note that lithological boundaries do not correspond to the knickpoints (Fig. 4). This is in agreement with the small difference in q_u of the bedrock, around several MPa, as discussed in Sect. 5.2. Another possible reason is sediment cover and tool effects (Yamanashi and Naruse, 2025). However, while the influence of the sediment requires further investigation, the cover and tool effects by riverbed gravel is considered to be insignificant for the target soft sedimentary rocks with q_u = 1–10 MPa.

https://doi.org/10.5194/egusphere-2026-290
Preprint. Discussion started: 4 February 2026

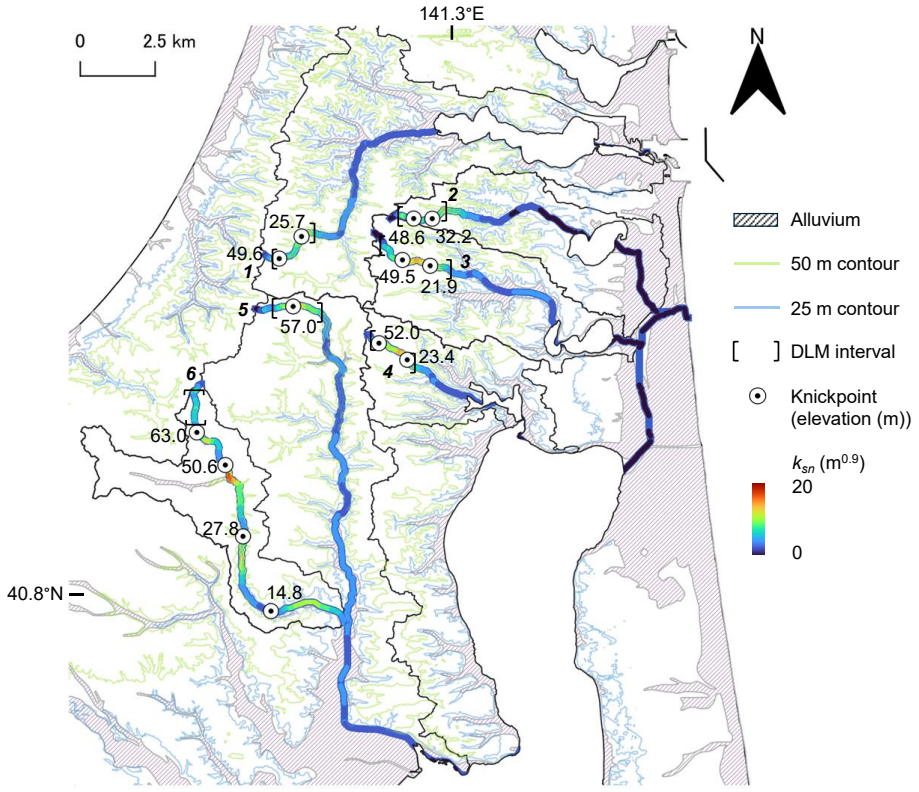

Figure 6: Knickpoints (points with elevation (m)) and 25 m and 50 m contours (blue and green lines). Color along the rivers demonstrates k_{sn}.

4.2 River incision parameters

We then compared the long-term river incision rate E and the river steepness k_{sn} based on log-bin averaged data (Fig. 7). Using the data of all the rivers, we confirmed that there is a positive correlation between E and k_{sn} with a correlation coefficient of R = 0.46. The parameter values were obtained as n of 1.54 [0.86, 2.22] (90% confidence interval) and K of 2.4×10^{-6} [5.6×10^{-7}, 1.0×10^{-5}] (m$^{0.1}$ y^{-1}).

Table 3 shows the parameter values obtained for each river. Although a relatively high correlation could be confirmed for rivers No. 3-6 ($R \geq 0.65$), values of K vary by almost nearly one order of magnitude. This variation may have been caused by the uncertainty of marine terrace surface z_t along the rivers; high-level marine terraces used for estimation of E (MIS 9 and MIS 11) are dissected by river and stream erosion (Fig. 2a). This can cause the large scatter in Fig. 7 for small incision rate, which correspond to upstream sections.

https://doi.org/10.5194/egusphere-2026-290
Preprint. Discussion started: 4 February 2026

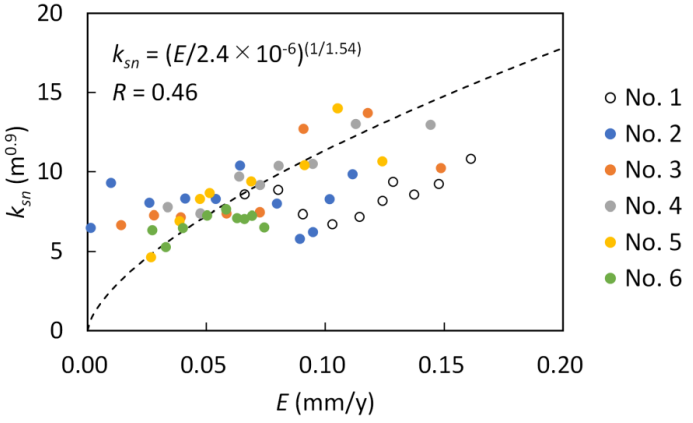

Figure 7: River incision rate versus channel steepness index k_{sn}.

Table 3: River incision parameters (n and K) and correlation coefficient estimated for each river.

No.	1	2	3	4	5	6
n (-)	0.82	1.14	2.10	1.59	1.48	2.07
K ($m^{0.1}$ y^{-1})	1.9×10^{-5}	3.7×10^{-6}	5.9×10^{-7}	2.5×10^{-6}	2.5×10^{-6}	1.0×10^{-6}
R	0.41	0.16	0.76	0.94	0.92	0.65

5 Discussions

5.1 The value of n

In Sect. 4.2, the results of n (= 1.54) show a nonlinear relationship between incision rate E and river steepness k_{sn}. This is consistent with previous research conducted in various regions, where most estimates of n are between 1 and 2 (e.g., Ouimet et al., 2009; DiBiase et al., 2010; Lague, 2014; Harel et al., 2016; Campforts et al., 2020; Gallen and Fernandez-Blanco, 2021; Leonard et al., 2023). Additionally, we confirmed that the target rivers are impacted by eustatic sea-level change.

The migration of fluvial knickpoints migration due to sea-level change can cause the nonlinearity ($n > 1$) (Pavano, 2025). To reduce the effect of sea-level change (i.e., fluctuation caused by the knickpoints), we compared k_{sn} and E averaged for each river in common with Pavano et al. (2016). As a result, an almost linear value of n = 1.01 was obtained (Fig. 8). In particular, the trend of rivers in the same basin (No. 2-6) are quite similar, with a correlation factor of R = 0.97. Even excluding river No.1, the estimated parameter value is similar: n = 1.02 [0.86, 1.18]. This suggests that past sea-level fluctuations may account for the nonlinear relationship between k_{sn} and E. Note that the neglected effect of channel width is limited, since parameter estimation was performed in the limited upstream and midstream areas (Fig. 6).

https://doi.org/10.5194/egusphere-2026-290
Preprint. Discussion started: 4 February 2026

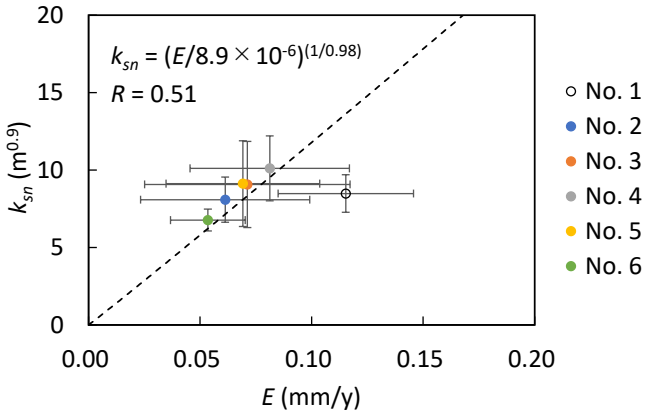

255 **Figure 8: River incision rate versus channel steepness index k_{sn} (averaged for each river section). Error bars denote ± 1 σ.**

5.2 The value of *K*

The value of K can vary by orders of magnitude due to lithology, climate, tectonics, hydraulic processes, and other environmental conditions (e.g., Murphy et al., 2016; Dibiase et al., 2018; Chen et al., 2019; Seybold et al., 2021). Among them, Haag and Schoenbohm (2025) confirmed a strong correlation ($R^2 = 0.89$) between global estimates for K based on ^{10}Be erosion
260 rates (Harel et al., 2016) and Schmidt hammer-derived lithologic erodibility ($K \propto L_E$, $L_E = q_u^{-2}$: Sklar and Dietrich, 2001; Turowski et al., 2023); where L_E is the lithologic erodibility (Campforts, 2020) and q_u is unconfined compressive strength (Fig. 9).

In this section, estimates for K for this study and the relationship between K and q_u in Haag and Schoenbohm (2025) were compared. In the study area, measured N-values from previously studies for each lithology are as follows (Onuma, 1972;
265 Planning Bureau, Ministry of Construction, Japan, 1997): 25–41 for the terrace deposits, 50–63 for the Hamada and Katchi formations, and 80–137 for the Takahoko formation. We then converted the N-values to q_u (q_u = 25–50 N MPa: Japanese Geotechnical Society, 2015): 0.6–2.0 MPa for the terrace deposits, 1.2–3.1 MPa for the Hamada and Katchi formations, and 2.0–6.8 MPa for the Takahoko formation. For the Hamada and Katchi formations of which the studied rivers mainly consist, estimated values are almost within the 90% confidence interval of the regression line of Haag and Schoenbohm (2025) (Fig.
270 9). Although rock strength in this study is out of range of the previous study (q_u = 10–100 MPa), a strong correlation was observed between the results of this study and the data in Haag and Schoenbohm (2025) with $R^2 = 0.85$. This highlights the significant influence of bedrock lithology on K, as indicated by previous research (e.g., Campforts et al., 2020; Haag and Schoenbohm, 2025).

However, the results of this study underestimate K (the regression line) in the work of Haag and Schoenbohm (2025). One
275 possible reason for this discrepancy is the effect of sea-level change, which is discussed in Sect. 5.1. When comparing the average k_{sn} and E in the river section, a larger K of 8.9×10^{-6} [4.7×10^{-7}, 1.7×10^{-4}] $m^{0.1}$ y^{-1} was obtained (Fig. 8). Although the estimation uncertainty is large, the estimated K value is consistent with the relationship described by Haag and Schoenbohm (2025). Another possible reason for the discrepancy is that we compared the present values of k_{sn} with long-term average erosion rates. Since the target rivers have been formed gradually by incising the flat marine terraces, long-term average k_{sn}
280 should be less than the present value. If the long-term average k_{sn} is half of present k_{sn}, the estimated K doubles without changing the n value.

https://doi.org/10.5194/egusphere-2026-290
Preprint. Discussion started: 4 February 2026

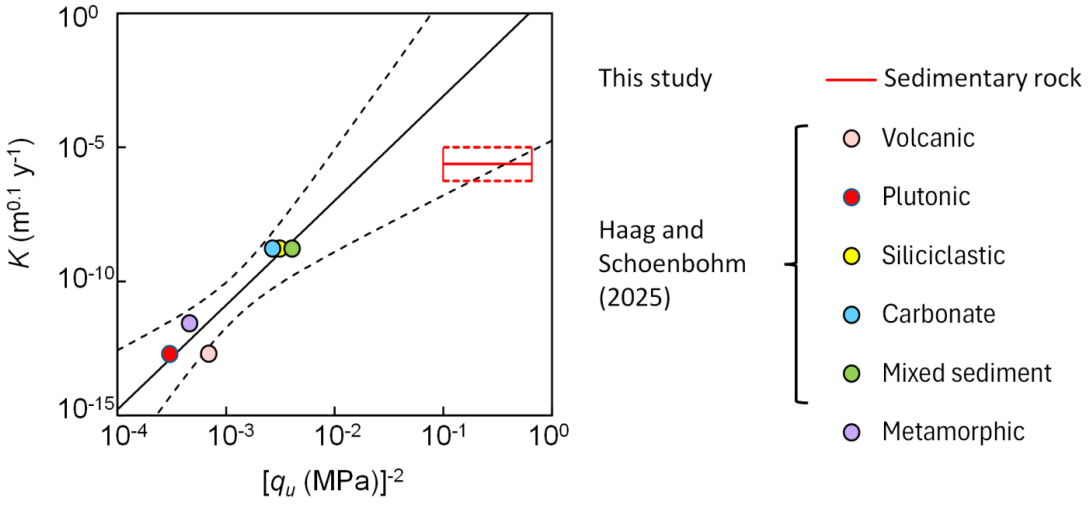

Figure 9: Comparison between the results of this study and data of Haag and Schoenbohm (2025) (color points) for unconfined compressive strength q_u and erosional coefficient K. The box plot shows the best estimate and 90% confidence interval of our results based on the log-bin averaged data for all the rivers. The black line and dashed lines are the best estimate and 90% confidence interval shown in Haag and Schoenbohm (2025).

6 Conclusions

This study estimated the river incision parameters for soft sedimentary rock, which are lacking in previous global compilations. The study targeted the Kamikita Coastal Plain, where bedrock lithology (sedimentary rocks of Miocene to Pleistocene) and uplift rate (approximately 0.2 mm y^{-1} over the past 300 ka) are assumed to be uniform. Parameter values were estimated using slope-area analysis based on river incision rates approximately derived from marine terraces (MIS 5e, 7, 9, and 11) widely distributed in the area. A summary of the main results is as follows.

(1) DL-like behaviour was confirmed in the limited upstream and midstream area ($A \geq 10^{-5}$ km^2) located upstream of the alluvium distribution for all rivers. Except for small rivers of $A < 25$ km^2, the concavity index m/n was between 0.35 and 0.6, which is the typical range for steady-state channels.

(2) Exponent n was nonlinear, ranging between 1 and 2, which is consistent with the previously global compilation. This nonlinearity can be due to past sea-level changes, causing knickpoints at similar elevations.

(3) For target rivers consisting mainly of late Pliocene and early Pleistocene sedimentary rock, erosion coefficient K was estimated to be $10^{-5\sim-6}$ $m^{0.1}$ y^{-1}. Estimated K is almost within 90% confidence interval of the previous global relationship with unconfined compressive strength q_u ($K \propto 1/q_u^2$). This supports the significance of bedrock lithology on K, as previously reported (e.g., Campfort et al. (2020) and Haag and Schoenbohm (2025)).

Although the estimation of long-term k_{sn} and E includes uncertainty (i.e., the formation age of river and the marine terrace surface), this study shows a similar trend of incision parameters for soft sedimentary rocks to more consolidated rocks in the previous global compilations. These results show the average trend of long-term erosion after MIS 9 or MIS 11. The obtained parameters are beneficial to perform predictions of long-term landscape evolution in the safety assessment of such as radioactive waste disposal. However, as we mentioned earlier, there is uncertainty due to the past sea-level change and the estimation error of marine terrace elevations. To further verify the estimated parameters, our next step will be the reproduction of past landscape evolution by numerical landscape evolution models using mixed DL and TL models.

https://doi.org/10.5194/egusphere-2026-290
Preprint. Discussion started: 4 February 2026

Data availability

The DEM data is available at Geospatial Information Authority of Japan (https://service.gsi.go.jp/kiban/). The geological data is available at National Institute of Advanced Industrial Science and Technology (https://gbank.gsj.jp/seamless/).

Author contributions

S. Takai and T. Sanga designed research. S. Takai and T. Sanga performed research and analyzed data. S. Takai wrote the original manuscript draft and led editing. All authors reviewed and revised the manuscript and approved the final version.

Competing interests

The authors declare that they have no conflict of interest.

Acknowledgements

The authors would like to thank Prof. T. Sugai of the University of Tokyo, Japan, for his valuable comments. This study was funded by the Secretariat of Nuclear Regulation Authority, Nuclear Regulation Authority, Japan.

Review statement

The review statement will be added by Copernicus Publications listing the handling editor as well as all contributing referees according to their status anonymous or identified.

References

Adams, B. A., Whipple, K. X., Forte, A. M., Heimsath, M., and Hodges, K.V.: Climate controls on erosion in tectonically active landscapes, Sci. Adv., 6, eaaz3166, https://doi.org/10.1126/sciadv.aaz3166, 2020.

AIST (National Institute of Advanced Industrial Science and Technology): The 2016 fiscal year project report of expenses for commission of safety review for geological disposal of radioactive waste: Evaluation methods toward safety review–geological information section, https://www.nsr.go.jp/data/000192112.pdf (last access: 5 December 2025), 2015 (in Japanese).

AIST (National Institute of Advanced Industrial Science and Technology): The 2017 fiscal year project report of expenses for commission of safety control for nuclear power plant facilities: Reconnaissance investigation for long-term prediction of natural disaster, https://www.nsr.go.jp/data/000186554.pdf (last access: 5 December 2025), 2016 (in Japanese).

AIST (National Institute of Advanced Industrial Science and Technology): Seamless digital geological map of Japan V2 1:200,000, Original edition, https://gbank.gsj.jp/seamless/ (last access: 5 December 2025), 2025.

Armitage, J. J., Whittaker, A. C., Zakari, M., and Campforts, B.: Numerical modelling of landscape and sediment flux response to precipitation rate change, Earth Surf. Dynam., 6, 77–99, https://doi.org/10.5194/esurf-6-77-2018, 2018.

Bishop, P., Hoey, T. B., Jansen, J. D., and Artza, I. L.: Knickpoint recession rate and catchment area: the case of uplifted rivers in Eastern Scotland, Earth Surf. Proc. Land., 778, 767–778, https://doi.org/10.1002/esp.1191, 2005.

Boulton, S. J.: Geomorphic response to differential uplift: River long profiles and knickpoints from Guandalcanal and Makira (Solomon Islands), Front. Earth Sci., 8, 10, https://doi.org/10.3389/feart.2020.00010, 2020.

Campforts, B. and Govers, G.: Keeping the edge: A numerical method that avoids knickpoint smearing when solving the stream power law, J. Geophys. Res.-Earth, 120, 1189–1205, https://doi.org/10.1002/2014JF003376, 2015.

https://doi.org/10.5194/egusphere-2026-290
Preprint. Discussion started: 4 February 2026

Campforts, B., Vanacker, V., Herman, F., Vanmaercke, M., Schwanghart, W., Tenorio, G. E., Willems, P., and Govers, G.: Parameterization of river incision models requires acoounting for environmental heterogeneity: insights from the tropical Andes, Earth Surf. Dynam., 8, 447–470, https://doi.org/10.5194/esurf-8-447-2020, 2020.

Chen, S. A., Michaelides, K., Grieve, S. W. D., and Singer, M. B.: Aridity is expressed in river topography globally, Nature, 573, 573–577, https://doi.org/10.1038/s41586-019-1558-8, 2019.

Desormeaux, C., Godard, V., Lague, D., Duclaux, G., Fleury, J., Benedetti, L., Bellier, O., and ASTER Team: Investigation of stochastic-threshold incision models across a climatic and morphological gradient, Earth Surf. Dynam., 10, 473–492, https://doi.org/10.5194/esurf-10-473-2022, 2022.

DiBiase, R. A., Rossi, M. W., and Neely, A. B.: Fracture density and grain size controls on the relief structure of bedrock landscapes, Geology, 46, 5, 399–402, https://doi.org/10.1130/G40006.1, 2018.

DiBiase, R. A., Whipple, K. X., Heimsath, A. M., and Ouimet, W. B.: Landscape form and millennial erosion rates in the San Gabriel Mountains, CA, Earth Planet. Sc. Lett., 289, 134–144, https://doi.org/10.1016/j.epsl.2009.10.036, 2010.

Duvall, A., Kirby, E., and Burbank, D.: Tectonic and lithologic controls on bedrock channel profiles and processes in coastal California, J. Geophys. Res., 109, F03002, https://doi.org/10.1029/2003JF000086, 2004.

Flint, J. J.: Stream gradient as a function of order, magnitude, and discharge, Water Resour. Res., 10, 969–973, https://doi.org/10.1029/WR010i005p00969, 1974.

Gailleton, B., Mudd, S. M., Clubb, F. J., Peifer, D., and Hurst, M. D.: A segmentation approach for the reproducible extraction and quantification of knickpoints from river long profiles, Earth Surf. Dynam., 7, 211–230, https://doi.org/10.5194/esurf-7-211-2019, 2019.

Gallen, S. F. and Fernandez-Blanco, D.: A new data-driven Bayesian inversion of fluvial topography clarifies the tectonic history of the Corinth Rift and reveals a channel steepness threshold, J. Geophys. Res.-Earth, 126, https://doi.org/10.1029/2020JF005651, 2021.

Haag, M. B. and Schoenbohm, L. M.: Thor: a rock strength database for investigating lithologic controls in landscape evolution, Earth Planet. Sc. Lett., 660, https://doi.org/10.1016/j.epsl.2025.119364, 2025.

Hack, J. T.: Studies of longitudinal stream profiles in Virginia and Maryland, U.S. Geol. Surv. Prof. Pap., 294–B, 1957.

Harel, M. A., Mudd, S. M., and Attal, M.: Global analysis of the stream power law parameters based on worldwide ^{10}Be denudation rates, Geomorphology, 268, 184–196, https://doi.org/10.1016/j.geomorph.2016.05.035, 2016.

Haviv, I., Enzel, Y., Whipple, K. X., Zilberman, E., Matmon, A., Stone, J., and Fifield, K., L.: Evolution of vertical knickpoints (waterfalls) with resistant caprock: Insights from numerical modeling, J. Geophys. Res.-Earth, 115, https://doi.org/10.1029/2008JF001187, 2010.

Henderson, F.: Open Channel Flow, MacMillan, New York, 522 pp., ISBN 9780023535109, 1966.

Hergarten, S.: Transport-limited fluvial erosion – simple formulation and efficient numerical treatment, Earth Surf. Dynam., 8, 841–854, https://doi.org/10.5194/esurf-8-841-2020, 2020.

Hilley, G. E., Porder, S., Aron, F., Baden, C. W., Johnstone, S. A., Liu, F., Sare, R., Steelquist, A., and Young, H. H.: Earth's topographic relief potentially limited by an upper bound on channel steepness, Nat. Geosci., 12, 828–832, https://doi.org/10.1038/s41561-019-0442-3, 2019.

Howard, A. D.: A detachment-limited model of drainage basin evolution, Water Resour. Res., 30, 2261–2285, https://doi.org/10.1029/94WR00757, 1994.

Howard, A. D. and Kerby, G.: Channel changes in badlands, Geol. Soc. Am. Bull., 94, 739–752, https://doi.org/10.1130/0016-7606(1983)94<739:CCIB>2.0.CO;2, 1983.

Hu, X., Zhang, Y., Guo, J., and Pan, B.: How does climate affect the topography in tectonically active orogens, Earth Surf. Proc. Land., 48, 1267–1280, https://doi.org/10.1002/esp.5547, 2023.

IAEA (International Atomic Energy Agency): Disposal of radioactive waste, Specific Safety Requirements No. SSR-5, 2011.

https://doi.org/10.5194/egusphere-2026-290
Preprint. Discussion started: 4 February 2026

Japan Meteorological Agency (JMA): Past weather data search, https://www.data.jma.go.jp/stats/etrn/index.php (last access: 19 January 2026) (in Japanese).

Japanese Geotechnical Society: Japan geotechnical society standard – Geothechnical and geoenvironmental investigation methods, Vol. 1, ISBN 9784886448231, 2015.

Kirby, E. and Whipple, K. X.: Quantifying differential rock-uplift rates via stream profile analysis, Geology, 29, 415–418, https://doi.org/10.1130/0091-7613(2001)029<0415:QDRURV>2.0.CO;2, 2001.

Kirby, E. and Whipple, K. X.: Expression of active tectonics in erosional landscapes, J. Struct. Geol., 44, 54–75, https://doi.org/10.1016/j.jsg.2012.07.009, 2012.

Koike, K. and Machida, H.: Altas of Quaternary Marine Terraces in the Japanese Islands, University of Tokyo Press, Tokyo, 105 pp., 2001.

Kudo, T.: Chronostratigraphy of the Lower to Middle Miocene in the eastern part of Shimokita Peninsula, Northeast Japan, Bull. Geol. Surv. Japan, 71, 5, 439–462, 2020 (in Japanese with English summary).

Kudo, T.: Cumulative volume step-diagram for eruptive magmas of Towada Volcano, Bull. Geol. Surv. Japan, 74, 3, 133–153, 2023 (in Japanese with English summary).

Kuwabara, T.: Relative sea-level changes and marine-terrace deposits in Kamikita plain, northern end of Honshu, Japan, J. Geol. Soc. Japan, 110, 2, 93–102, https://doi.org/10.5575/geosoc.110.93, 2004 (in Japanese with English summary).

Kuwabara, T.: Fission-track dating of the middle-pleistocene shirobeta tephra (WP) in the Kamikita Plain, northeast Japan, Quat. Res. Jpn., 46, 5, 433–436, https://doi.org/10.4116/jaqua.46.433, 2007 (in Japanese).

Kuwabara, T.: Environmental change and its correlation to terraces based on phytolith assemblage of tephra-soil succession after the later half of the middle Pleistocene drilled on the Kamikita Plain, NE Japan, Quat. Res. Jpn., 48, 6, 405–416, https://doi.org/10.4116/jaqua.48.405, 2009 (in Japanese with English summary)

Lague, D.: The stream power river incision mode: evidence, theory and beyond, Earth Surf. Proc. Land., 39, 38–61, https://doi.org/10.1002/esp.3462, 2014.

Leonard, J. S., Whipple, K.X., and Heimsath, A. M.: Controls on topography and erosion of the north-central Andes, Geology, 52, 2, 153–158, https://doi.org/10.1130/G51618.1, 2023.

Liu, Z., Han, L., Boulton, S. J., Wu, T., and Guo, J.: Quantifying the transient landscape response to active faulting using fluvial geomorphic analysis in the Qianhe Graben on the southwest margin of Ordos, China, Geomorphology, 351, 106974, https://doi.org/10.1016/j.geomorph.2019.106974, 2020.

Marder, E. and Gallen S. F.: Climate control on the relationship between erosion rate and fluvial topography, Geology, 51, 5, 424–427, https://doi.org/10.1130/G50832.1, 2023.

Matsu'ura, T., Komatsubara, J., and Wu, C.: Accurate determination of the Pleistocene uplift rate of the NE Japan forearc from the buried MIS 5e marine terrace shoreline angle, Quat. Sci. Rev., 212, 45–68, https://doi.org/10.1016/j.quascirev.2019.03.007, 2019.

METIJ (Ministry of Economy, Trade and Industry of Japan): Nationwide Map of "Scientific Features" relevant for Geological Disposal, https://www.numo.or.jp/en/jigyou/Nationwide_Map_of_Scientific_Features.pdf (last access: 5 December 2025), 2017 (in Japanese).

Miyauchi, T.: Quaternary crustal movements estimated from deformed terraces and geologic structures of the Kamikita coastal plain, northeast Japan, Geogr. Rev. Jpn., 58, 8, 492–515, https://doi.org/10.4157/grj1984a.58.8_492, 1985 (in Japanese with English summary).

Montgomery, D. R. and Foufoula-Georgiou, E.: Channel network source representation using digital elevation models, Water Resour. Res., 29, 12, 3925–3934, https://doi.org/10.1029/93WR02463, 1993.

Murphy, B. P., Johnson, J. P. L., Gasparini, N. M., and Sklar L. S.: Chemical weathering as a mechanism for the climatic control of bedrock river incision. Nature, 532, 223–227, https://doi.org/10.1038/nature17449, 2016.

https://doi.org/10.5194/egusphere-2026-290
Preprint. Discussion started: 4 February 2026

NUMO (Nuclear Waste Management Organization of Japan): The NUMO Pre-siting SDM-based Safety Case, NUMO-TR-21-01, 2021.

Ogami, T.: Dynamics of longitudinal river profiles associated with knickpoints since the Middle Pleistocene on the northern Sanriku Coast, NE Japan, The Quaternay Research (Daiyonki-Kenkyu), 54, 3, 113–128, https://doi.org/10.4116/jaqua.54.113, 2015 (in Japanese with English summary).

Onuma, Z.: Geological character of Mutsu-Ogawara area Aomori prefecture, Jour. Japan Soc. Eng. Geol., 13, 1, 8–22, https://doi.org/10.5110/jjseg.13.8, 1972 (in Japanese with English summary).

Ott, R. F., Perez-Consuegra, N., Scherler, D., Mora, A., Huppert, K. L., Braun, J., Hoke, G. D., and Sandoval Ruiz, J. R.: Erosion rate maps highlight spatio-temporal patterns of uplift and quantify sediment export of the Northern Andes. Earth Planet. Sc. Lett., 621, 118354, https://doi.org/10.1016/j.epsl.2023.118354, 2023.

Ouimet, W. B., Whipple, K. X., and Granger, D. E.: Beyond threshold hillslopes: Channel adjustment to base-level fall in tectonically active mountain ranges, Geology, 37, 7, 579–582, https://doi.org/10.1130/G30013A.1, 2009.

Pavano, F.: Fault geometry, strain partitioning and deformation history inferred by fluvial topography and marine terrace analyses, Geomorphology, 472, https://doi.org/10.1016/j.geomorph.2024.109583, 2025.

Pavano, F., Pazzagila, F. J., and Catalano, S.: Knickpoints as geomorphic markers of active tectonics: A case study from northeastern Sicily (southern Italy), Lithosphere, 8, 6, 633–648, https://doi.org/10.1130/L577.1, 2016.

Perron, J. T. and Royden, L.: An integral approach to bedrock river profile analysis, Earth Surf. Proc. Land., 38, 570–576, https://doi.org/10.1002/esp.3302, 2013.

Planning Bureau, Ministry of Construction, Japan: General description of the ground in the Hachinohe and Misawa areas in Aomori prefecture, 1997 (in Japanese).

Seybold, H., Berghuijs, W. R., Prancevic, J. P., and Kirchner, J. W.: Global dominance of tectonics over climate in shaping river longitudinal profiles, Nat. Geosci., 14, 503–507, https://doi.org/10.1038/s41561-021-00720-5, 2021.

Sklar, L. S. and Dietrich, W. E.: Sediment and rock strength controls on river incision into bedrock, Geology, 29, 12, 1087–1090, https://doi.org/10.1130/0091-7613(2001)029<1087:SARSCO>2.0.CO;2, 2001.

Snyder, N. P., Whipple, K. X., Tucker, G. E., and Merritts, D. J.: Landscape response to tectonic forcing: Digital elevation model analysis of stream profiles in the Mendocino triple junction region, northern California, Geol. Soc. Am. Bull., 112, 8, 1250–1263, https://doi.org/10.1130/0016-7606(2000)112<1250:LRTTFD>2.0.CO;2, 2000.

Snyder, N. P., Whipple, K. X., Tucker, G. E., and Merritts, D. J.: Interactions between onshore bedrock-channel incision and nearshore wave-base erosion forced by eustasy and tectonics, Basin Res., 14, 2, 105–127, https://doi.org/10.1046/j.1365-2117.2002.00169.x, 2003.

Stock, J. and Dietrich, W. E.: Valley incision by debris flows: Evidence of a topographic signature, Water Resour. Res., 39, 4, https://doi.org/10.1029/2001WR001057, 2003.

Stock, J. D., Montgomery, D. R., Collins, B. D., Dietrich, W. E., and Sklar, L.: Field measurements of incision rates following bedrock exposure: implications for process controls on the long profiles of valleys cut by rivers and debris flows, Geol. Soc. Am. Bull., 117, 174–194, https://doi.org/10.1130/B25560.1, 2005.

STUK (Radiation and Nuclear Safety Authority): Disposal of nuclear waste: Guide YVL D.5, STUK, Helsinki, Finland, 2013.

Takahashi, N. O., Shyu, J. B. H., Toda, S., Matsushi, Y., Ohta, R. J., and Matsuzaki, H.: Transient Response and Adjustment Timescales of Channel Width and Angle of Valley-Side Slopes to Accelerated Incision, J. Geophys. Res.-Earth, 128, 8, e2022JF006967, https://doi.org/10.1029/2022JF006967, 2023.

Tarboton, D. G., Bras, R. L., and Rodriguez-Iturbe, I.: On the extraction of channel networks from digital elevation data, Hydrol. Process., 5, 81–100, https://doi.org/10.1002/hyp.3360050107,1991.

Turowski, J. M., Prub, G., Voigtlander, A., Ludwig, A., Landgraf, A., Kober, F., and Bonnelye, A.: Geotechnical controls on erodibility in fluvial impact erosion, Earth Surf. Dynam., 11, 979–994, https://doi.org/10.5194/esurf-11-979-2023, 2023.

https://doi.org/10.5194/egusphere-2026-290
Preprint. Discussion started: 4 February 2026

Vanacker, V., Blanckenburg, F. V., Govers, G., Molina, A., Campforts, B., and Kubik, P. W.: Transient river response, captured by channel steepness and its concavity, Geomorphology, 228, 234–243, https://doi.org/10.1016/j.geomorph.2014.09.013, 2015.

Wang, Y., Zhang, H., Zheng, D., Yu, J., Pang, J., and Ma, Y.: Coupling slope-area analysis, integral approach and statistic tests to steady-state bedrock river profile analysis, Earth Surf. Dynam., 5, 145–160, https://doi.org/10.5194/esurf-5-145-2017, 2017.

Whipple, K. X.: Bedrock rivers and the geomorphology of active orogens, Annu. Rev. Earth. Pl. Sc., 32, 151–185, https://doi.org/10.1146/annurev.earth.32.101802.120356, 2004.

Whipple, K. X., DiBiase, R., and Crosby, B.: 9.28 Bedrock Rivers, vol. 9, 550–573, ISBN 9780080885223, https://doi.org/10.1016/B978-0-12-374739-6.00254-2, 2013.

Whipple, K. X. and Tucker, G. E.: Dynamics of the stream-power river incision model: Implications for height limits of mountain ranges, landscape response timescales, and research needs, J. Geophys. Res., 104, 17661–17674, https://doi.org/10.1029/1999JB900120, 1999.

Whipple, K. X. and Tucker, G. E.: Implications of sediment-flux-dependent river incision models for landscape evolution. J. Geophys. Res., 107, B2, 2039, https://doi.org/10.1029/2000JB000044, 2002.

Whipple, K. X., Wobuc, C., Crosby, B., Kirby, E., and Sheehan, D.: New tools for quantitative geomorphology: extraction and interpretation of stream profiles from digital topographic data, GSA Short Course, 506, 1–26, 2007.

Wobus, C., Whipple, K. X., Kirby, E., Snyder, N., Johnson, J., Spyropolou, K., Crosby, B., and Sheehan, D.: Tectonics from topography: procedures, promise, and pitfalls, in Tectonics, Climate, and Landscape Evolution, Geological Society of America, 398, 55–74, https://doi.org/10.1130/2006.2398(04), 2006.

Yamanashi, N. and Naruse, H.: Limited influence of bedrock strength on river profiles: the dominant role of sediment dynamics, EGUsphere [preprint], https://doi.org/10.5194/egusphere-2025-4283, 2025.